Full Length Article

High temperature formability of graphene nanoplatelets-AZ31 composites fabricated by stir-casting method

Muhammad Rashad [a,b,*], Fusheng Pan [a,b,c,*], Yanglu Liu [a,b], Xianhua Chen [a,b], Han Lin [a,b], Rongjian Pan [a,b], Muhammad Asif [d], Jia She [e]

[a] College of Materials Science and Engineering, Chongqing University, Chongqing 400044, China
[b] National Engineering Research Center for Magnesium Alloys, Chongqing University, Chongqing 400044, China
[c] Chongqing Academy of Science and Technology, Chongqing 401123, China
[d] School of Materials Science and Engineering, Dalian University of Technology, Dalian 116024, China
[e] Nuclear Power Institute of China, Chengdu 610213, China

Abstract

Outstanding mechanical properties of graphene nanoplatelets (GNPs) make them ideal reinforcement for mass production of composites. In this research, the composites were fabricated by stir-casting method. GNPs were added in 1.5 and 3.0 wt.% into Mg–3wt.% Al–1wt.% Zn (AZ31) magnesium alloy. As cast ingots were preheated for one hour and extruded at 350 °C with extrusion ratio of 5.2:1. As extruded AZ31-GNPs composites were micro-structurally characterized with X-ray diffraction, optical microscopy and scanning electron microscopy. Vickers micro-hardness of synthesized materials was investigated both in parallel and perpendicular to extrusion directions. Room temperature mechanical testing revealed that with increasing GNP's content, tensile fracture strain was remarkably increased without significant compromise in tensile strength. Furthermore, as extruded AZ31-3GNPs composites were subjected to tensile testing at temperatures ranging from 75 °C to 300 °C with initial strain rate of $2 \times 10^{-3} \, \text{s}^{-1}$ to evaluate high temperature formability of composite. It was found that like CNTs, GNPs also have the potential to sustain tensile strength at high temperatures.
© 2016 Production and hosting by Elsevier B.V. on behalf of Chongqing University. This is an open access article under the CC BY-NC-ND license (http://creativecommons.org/licenses/by-nc-nd/4.0/).

Keywords: Metal matrix composites; Mechanical properties; Stir-casting method; Elevated temperatures

1. Introduction

The world is facing energy crises and the demand for light-weight materials is increasing day by day. Among the lightweight structural materials, magnesium (density of 1.74 g/cm³) and its alloys are considered the most promising materials in automotive and aerospace industries. Additionally, magnesium based composites and alloys also reveal good machinability, castability, damping properties and thermal stability. However, magnesium based composites and alloys are not as strong as aluminum alloys. For further utilization of magnesium based materials, improvement in their room and elevated temperature mechanical properties is very necessary. In recent years, several reinforce-ments (i.e. Ti, CNTs, SiC, TiO₂, Al₂O₃, and Cu) have been used to enhance the mechanical properties of magnesium alloys [1–5]. Among these reinforcements, ceramic particles contribute toward high hardness and Young's modulus with significant decrease in elongations of resulting composite. This might be attributed to poor wettability between magnesium matrix and reinforcements. The composites with carbon nanotubes (CNTs) reinforcements are facing problems of poor dispersion of rein-forcements, which prohibit their use on industrial scale.

In recent years, graphene and its derivatives have been exten-sively used to enhance the mechanical properties of polymer composites [6]. Graphene can be used as multilayer graphenes which are known as graphene nanoplatelets (GNPs). GNPs have several advantages over CNTs due to their two dimen-sional morphology. Since the mechanical strength of GNPs is comparable to that of CNTs, several attempts have been made to synthesize metal composites reinforced with GNPs [7]. Recently, Pan's group [8–13] has made successful attempts to

* Corresponding authors. College of Materials Science and Engineering, Chongqing University, Chongqing 400044, China. Fax: +86 23 67300077.
E-mail addresses: rashadphy87@gmail.com (M. Rashad); fspan@cqu.edu.cn (F. Pan).

fabricate GNPs reinforced magnesium, aluminum, and their alloys via powder metallurgy method. Experimental results revealed significant improvement in room and elevated temperature mechanical properties of resulting composites. Furthermore, it was found that GNPs exhibit good wettability with aluminum as compared with magnesium metal.

Generally, magnesium reveals poor formability and strength at elevated temperatures. To overcome these difficulties, several researchers have explored creep resistance and high temperature strength of different composites. For example, Wenwen et al. [14] synthesized AZ91–3% La–0.3% Ca alloy to investigate its creep resistance and high temperature strength. Khomamizadeh et al. [15] found that AZ91–2% RE magnesium alloy could retain its yield strengths at 140 °C. Additionally, CNTs [16] and Al2O3 [17] reinforcements were found to be effective in improvement of formability of AZ31 magnesium alloys. In 2015, Rashad et al. [18] synthesize AZ61 alloy reinforced with GNPs. The tensile strength of as extruded graphene nanoplatelets-AZ61 composite was investigated at temperatures ranging from 75 °C to 225 °C. The results showed that total fracture strain increases and tensile yield strength decreases with increasing testing temperature. However, literature review revealed that formability of AZ31 alloy reinforced with graphene nanoplatelets has never been reported.

Accordingly, in present work, (1.5, 3.0) wt.% GNP reinforced Mg–3wt.% Al–1wt.% Zn (AZ31) nanocomposites were synthesized via stir-casting method followed by hot extrusion. The microstructural and mechanical properties of nanocomposites were investigated and compared with un-reinforced AZ31 alloy. Additionally, composites were subjected to high temperature tensile loading to evaluated high temperature formability of synthesized materials.

2. Experimental procedures

2.1. Synthesis of composites

Pure Mg, Al ingots and Zn granular were used to fabricate Mg–3wt.% Al–1wt.% Zn (AZ31) alloy which was used as matrix. Graphene nanoplatelets with thickness and average diameter of 15–20 nm and 5–10 μm respectively, supplied from Chengdu Organic Chemistry Co. Ltd., China, were used as reinforcement particles.

The details of synthesis procedure were described in Reference [18]. Stir casting method was used to synthesize GNPs reinforced AZ31 alloy composites. In the first step, about 1.3 Kg Mg ingot was melted at 740 °C under CO2-SF6 protective atmosphere in a graphite crucible using an electrical resistance furnace. Then, Al (3wt.%) and granular Zn (1wt.%) were added into Mg melt. In the second step, GNPs powder was added into AZ31 alloy molten slurry and mixture was stirred for 1.0 min. As-stirred mixture was reheated to 740 °C and kept at 740 °C for 10 minutes. The composite mixture was poured into a steel mold and allowed to solidify normally. The casted billets were cut into Φ82mm × 45 mm samples. Billets were hot extruded using a 500T hydraulic press at 350 °C with an extrusion ratio of 5.2:1 to obtain the rods of 16 mm diameter. The RAM speed was set at 1m/min.

2.2. Characterizations of materials

Samples, machined from extruded bars were polished and characterized for their microstructures. X-ray diffraction method was adopted to investigate the presence of different peaks related to Mg, Al, Zn, GNPs and their intermetallic phases. X-ray diffraction (XRD) analysis were conducted on extruded bulk samples using a Rigaku D/MAX-2500PC diffract meter with Cu Kα radiation at 40KV and 30 mA, and a scan rate of 0.02° s^{-1} in a 2θ range of 10–90°. Furthermore, diffractometer with Cu-Ka radiation at 40KV and 34 mA was used to analyze crystallographic textures of AZ31 alloy and its composites reinforced with GNPs. Surface analysis of fabricated materials were carried out using optical microscopy and scanning electron microscopy (SEM) equipped with energy dispersive spectroscopy (EDS). Digital micro-hardness tester (Shanghai HX-1000TM) was used to measure the microhardness under a load of 100 grams and 15 seconds dwell time. Hardness was measured both in parallel and perpendicular to extrusion directions. Tensile samples with 25 mm gauge length and 5 mm diameter were machined along extrusion directions. Similarly, compression samples with 12 mm height and 8 mm diameter were machined, and tests were carried out on bulk samples parallel to extrusion directions with strain speed of $1 \times 10^{-3}\,s^{-1}$. High temperature tensile tests were carried out for AZ31-3GNP composite at temperatures ranging from 75 °C to 300 °C with initial strain rate of $2 \times 10^{-3}\,s^{-1}$. Tensile and compression fracture surfaces were investigated using SEM to understand various possible mechanisms.

3. Results and discussions

3.1. X-ray diffraction and crystallographic texture measurements

Fig. 1 shows X-ray diffraction patterns of as extruded AZ31 alloy and its composites reinforced with GNPs. Mostly, peaks corresponding to pure Mg were observed in all samples, revealing no phase formation occur between GNPs and AZ31 alloy
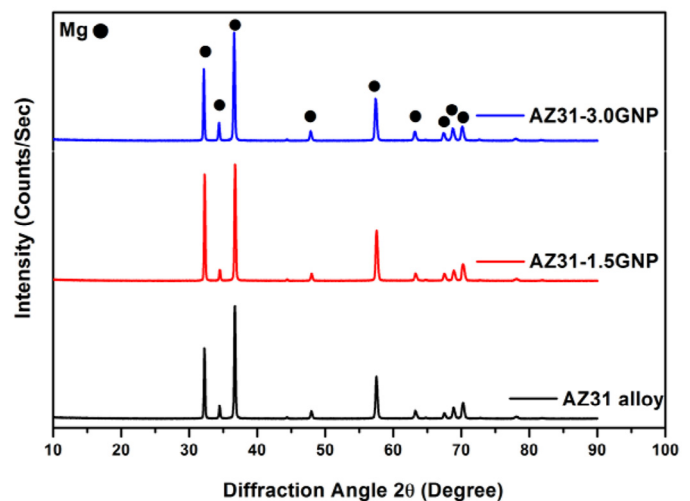

Fig. 1. X-ray diffraction patterns of as-extruded AZ31 alloy and its composites taken in transverse direction of the samples.
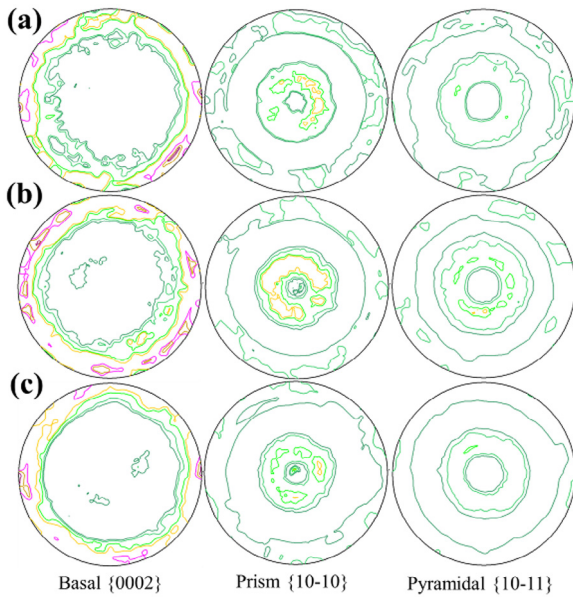
Fig. 2. Pole figures {0002}, {10$\bar{1}$0}, and {10$\bar{1}$1} of as-extruded (a) AZ31 alloy, (b) AZ31-1.5GNP composite, and (c) AZ31-3GNP composite taken along the cross section direction of the samples.

Fig. 3. Optical images showing grain morphology of as-extruded (a) AZ31 alloy, (b) AZ31-1.5GNP composite, and (c) AZ31-3GNP composite.

[18]. This may be attributed to low weight fraction of GNPs in composite matrix. According to Mg-Al phase diagram, $Mg_{17}Al_{12}$ intermetallic phase should be present in all samples; however no peak was traced due to its low contents.

Fig. 2 revealed crystallographic texture analysis of AZ31 alloy and its composites taken along cross section direction of the samples. Pole figures, basal {0002}, prism {10$\bar{1}$0}, and pyramidal {10$\bar{1}$1} were measured along 360°. Room temperature mechanical properties of magnesium alloys and composites are related to basal plane activity which depends on crystalline alignment via Schmidt factor [19]. Therefore, changes in mechanical properties of synthesized materials depend on crystallographic texture difference between pure matrix and composite material. Crystallographic texture observation revealed that basal texture intensity is distributed along the periphery in case of pure AZ31 alloy. However, in case of composites with 1.5 and 3.0 wt.% GNPs, the basal texture intensity distribution is changed to certain extent, i.e. spreads toward centers. The changes in basal texture intensities between AZ31 alloy and composites witness the changes in room temperature strength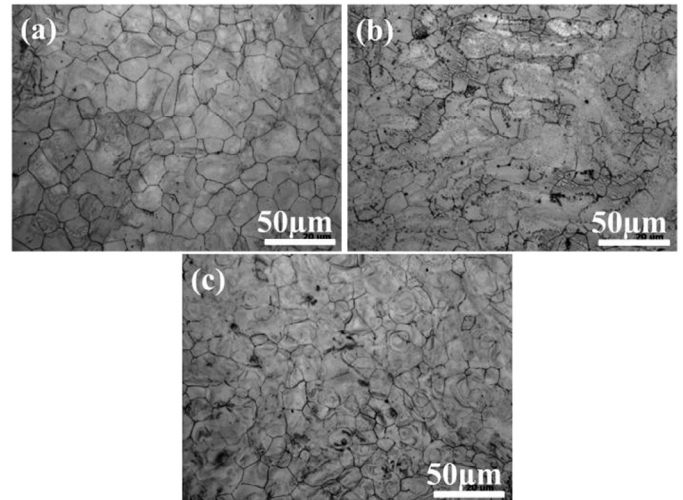 of composites. Furthermore, it can be observed that prismatic and pyramidal texture intensities of pure alloy and composites were also changed to a small extent.

3.2. Microstructural characterization

Fig. 3 shows grain morphology of pure AZ31 alloy and its composites in as extruded state. It can be seen that pure AZ31 alloy exhibits grain size of 12 ± 3 µm. While the composites with 1.5 and 3.0 wt.% GNPs revealed the grain size of 11 ± 4 µm and 11 ± 3 µm respectively. No significant changes were observed in grain size when considering the standard deviations. Thus, it can be concluded that the influence of GNP addition is minimal on grain size coarsening and reduction. It is known that particle stimulated grain nucleation occur only for particle size less than 1 µm [20,21]. However, in the present study, GNPs size is greater than 1 µm and fine grains were observed near GNP particles and agglomerates as shown in Fig. 3. It means that agglomerated particles have an active role in grain boundary pining than individual or nanoparticles [20,21].

Scanning electron microscopic images of extruded pure AZ31 alloy and its composites are shown in Fig. 4. It can be seen that microstructural surfaces of all materials are very clear and free of pores which witness the potentiality of stir casting method. SEM images also revealed small changes in grain size
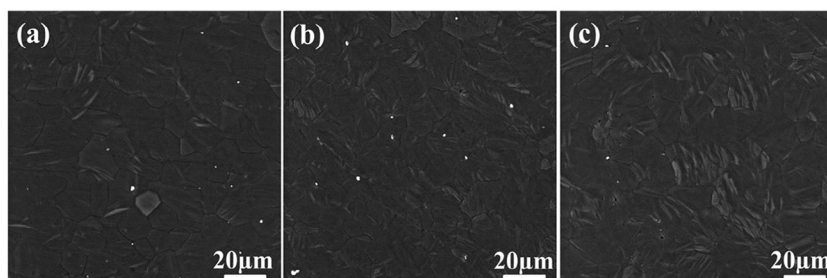

Fig. 4. SEM images of as-extruded (a) AZ31 alloy, (b) AZ31-1.5GNP composite, and (c) AZ31-3GNP composite.
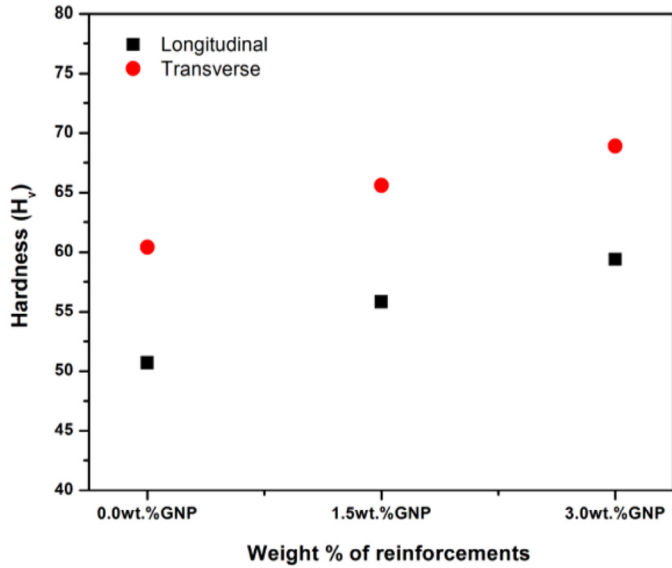
Fig. 5. Vickers hardness of extruded AZ31 alloy and its composites in transverse and longitudinal directions.

(white particles) as shown in Fig. 4. It is known that GNPs may help to dissolve $Mg_{17}Al_{12}$ phases and affect their growth in composite matrix [9]. The same phenomenon was observed in composite with relatively higher weight content (3.0) of GNPs as shown Fig. 4 (c). The AZ31-3GNPs composite surface revealed fewer $Mg_{17}Al_{12}$ particles as compared to pure AZ31 alloy and AZ31-1.5GNPs composite.

3.3. Room temperature mechanical properties

Micro-hardness results of as extruded AZ31 alloy and its composites measured in transverse and longitudinal directions are shown in Fig. 5. It can be observed that Vickers hardness of materials in transverse direction is higher than in longitudinal directions. It can also be observed that addition of GNPs and its increasing contents leads to increase in Vickers hardness. The AZ31-3GNP composite exhibits the highest value of hardness ($H_v = 68.9$). Thus, GNPs may contribute toward increased micro-hardness of AZ31 alloy. In the previous work, GNPs have also shown significant potential to increase the micro-hardness of AZ31 alloy fabricated by powder metallurgy method [9]. The increased micro-hardness of composites maybe attributed to presence of high hardness GNP particles and constraint to localized deformation during indentation.

Fig. 6 and Table 1 represent room temperature tensile and compression properties of AZ31 alloy and its composites reinforced with GNPs. The significant improvement in mechanical properties was observed. The tensile fracture strain and

between pure AZ31 alloy and its composites. The α-Mg and $Mg_{17}Al_{12}$ intermetallic phases can be observed in all materials. According to Mg-Al phase diagram, Mg and Al will react with each other during cooling when temperature is less than 460°C. This reaction may lead to formation of $Mg_{17}Al_{12}$ particles
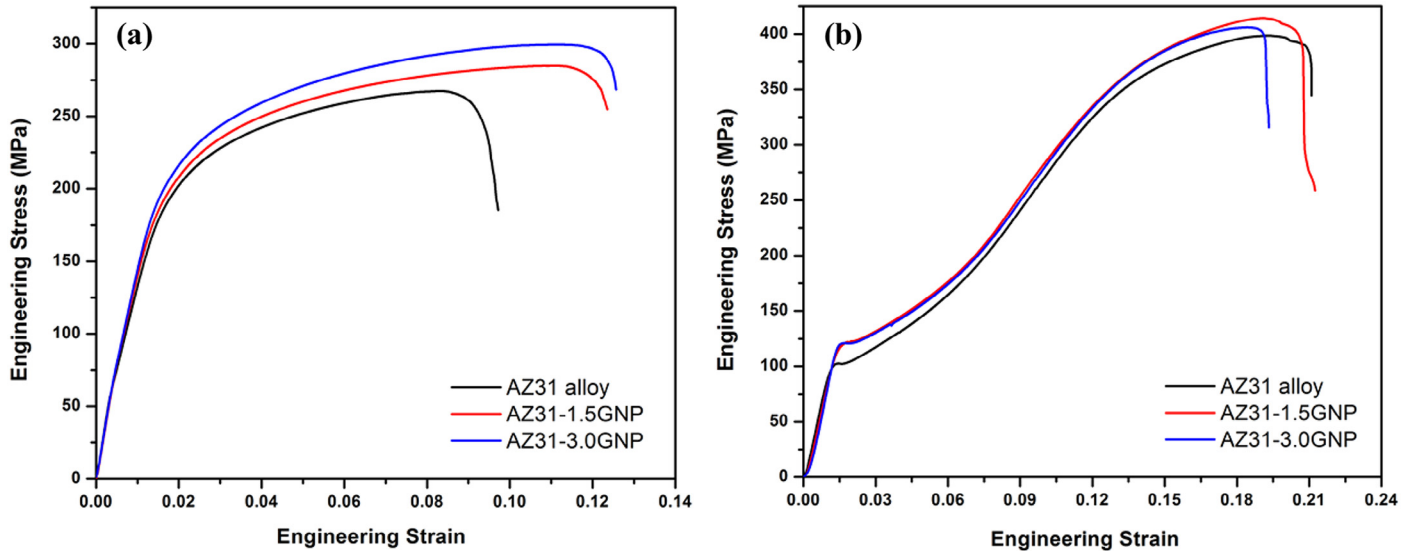

Fig. 6. Room temperature tensile (a) and compression (b) stress–strain curves of AZ31 alloy and its composites.

Table 1
Room temperature tensile and compression properties of AZ31 alloy and its composites.

Materials	Tensile properties			Compressive properties		
	0.2% YS (MPa)	UTS (MPa)	FS (%)	0.2% YS (MPa)	UCS (MPa)	FS (%)
AZ31 Alloy	183 ± 4.3	267 ± 6.5	09.74 ± 1.5	100 ± 3.3	398 ± 5.1	21.0 ± 1.4
AZ31-1.5GNP	187 ± 3.5	284 ± 5.4	12.34 ± 3.4	121 ± 4.7	415 ± 3.4	21.2 ± 2.1
AZ31-3GNP	195 ± 4.5	299 ± 6.2	12.56 ± 4.3	120 ± 2.8	406 ± 4.1	19.3 ± 1.8

YS: Yield strength; UTS: Ultimate tensile strength; FS: Fracture strain; UCS: Ultimate compressive strength.

compression yield strength were improved by 28.95% and 21% respectively, with addition of GNPs. The improvement in mechanical properties of composites may be attributed to (a) Hall-Petch model, (b) load transfer mechanism related to platelet pull-out strengthening, (c) dislocation densities related to coefficient of thermal expansion mismatch between GNPs and alloy matrix, and (c) Orowan looping related to GNP particle distribution.

The Hall-Petch model [22,23] can be described in terms of grain refinement $\sigma_c = \sigma_0 + K(d)^{-\frac{1}{2}}$. Where σ_c is yield strength of composite materials, σ_0 and K are constant related to material, and d is the mean grain size. In the present study, no significant changes were observed in grain size of AZ31 and GNPs reinforced composites. Therefore, the contribution in mechanical strength due to Hall-Petch model can be ignored. Generally, for the composites reinforced by fiber, nano-sheets or platelets, load can be shifted from soft matrix to reinforcements (fiber, sheets, or platelets) through sheer stress created along matrix/reinforcement interface [24,25]. This may result in variable stress along the GNPs (reinforcement particles in present study). The stress on GNPs increases proportionally from GNPs' end to reach a maximum value at the central region. It will cause pulling-out/pulling-off of GNPs inside the composite matrix. The pulling-out/pulling-off depends on (a) orientation and wettability of GNPs inside composite matrix and (b) matrix strength. Orientation of GNP particles plays a vital role in improving mechanical strength. The GNPs embedded along tensile direction will elongate (depending on their strength) and resist against rupture. However, GNPs embedded in perpendicular directions will not contribute significantly. The wettability of GNPs with Mg matrix is a crucial factor affecting the potentiality of reinforcements. The alloys containing large amount of Al may results in good compatibility between GNPs and alloy matrix. The composites yield strength due to load transfer can be estimated using modified shear-lag model [9] as given bellow.

$$\sigma_{composite} = V_{rein}\left(\frac{S}{A}\right)\left(\frac{\tau_m}{2}\right) + \sigma_{matrix}V_{matrix} \qquad (1)$$

where V_{rein} and V_{matrix} are volume fraction of reinforcements and matrix. S and A are interfacial and cross-sectional area of graphene nanoplatelets or carbon nanotubes respectively. τ_m is the shear strength of magnesium matrix and approximately equal to $\sigma_{matrix}/2$.

The coefficient of thermal expansion for graphene nanoplatelets is $10^{-6}\,K^{-1}$. On the other hand, coefficient of thermal expansion for magnesium, aluminum and zinc are $25 \times 10^{-6}\,K^{-1}$, $22.2 \times 10^{-6}\,K^{-1}$, and $16.6 \times 10^{-6}\,K^{-1}$ respectively. In addition, elastic modulus (E) of graphene nanoplatelets ranges between 0.7 and 1.2 TPa and that for AZ31 alloy it is about 45 GPa [5]. Thus, great differences exist between coefficient of thermal expansion and elastic modulus of matrix and reinforcement particles. This mismatch may lead to formation of dislocations at the interface. These dislocations will resist the fracture under tensile or compression loading, thus leading to increased strength of composites [26]. Orowan looping mechanism [13] also plays an

important role in improving mechanical properties of composites. This mechanism is governed by restricted movement of dislocations produced due to presence of reinforcement particles (GNPs). Additionally, dispersion of GNPs is also important to have as many particles as possible to involve in increasing the strength.

Recently, a comparative study between GNPs and CNTs was carried out in AZ31 magnesium alloy matrix using powder metallurgy method [9]. Ball milling technique was used to disperse 0.3 wt.% GNPs in AZ31 alloy powders under Ar gas atmosphere. Although, experimental results revealed uniform dispersion of GNPs in composites, GNP structures were damaged during ball milling technique as shown by Raman spectroscopy results. Mechanical properties testing results revealed significant improvement in tensile fracture strain. No significant improvement in compression strength was observed which may be due to buckling nature of GNPs. Comparison of previous study with present work confirmed the enhancement potential of GNPs in AZ31 alloy which is almost same. However, if we compare the present work with Ref. [18], we found that GNPs are sensitive to content of Al in magnesium alloy matrix. In AZ61-GNPs composite, tensile/compression yield strengths were increased with slight decrease in fracture strains. This may be caused by formation of Al_4C_3 in composite matrix.

3.4. Fracture images

Fig. 7 shows tensile and compression fracture surfaces of extruded AZ31 alloy and its composites reinforced with GNPs. It can be observed that for all materials, tensile fracture surfaces revealed dimples and tear ridges. The composite tensile surfaces revealed some regions where GNPs were aligned along tensile directions. The GNPs were pulled-out/pulled-off during tensile loading, thus significant load was transferred from soft matrix to hard GNPs, which resulted in increased tensile fracture strain values. On the other hand, compression fracture surfaces revealed existence of shear bands in AZ31 alloy as well as in composites. It can be seen that for all materials, fracture occurred at 45° degree with respect to loading direction.

3.5. High temperature deformation behavior of AZ31-3GNP composite

Fig. 8 and Table 2 show high temperature tensile properties of AZ31-3GNPs composites. It can be seen that with increase in testing temperature, GNP particles have considerably exacerbated the softening of AZ31 alloy matrix. High temperature analysis revealed that curves up to 150°C are governed by work-hardening. The yield strength of composites decreases with increase in testing temperatures. Increasing temperature from 150 to 225°C, there is remarkably reduction in yield stress. With further increase in temperature from 225° to 300°C, there is abrupt fall in yield stress. The AZ31-3GNPs composite is thermally stable up to 150°C. The dramatic softening at 300°C may be attributed due to recrystallization and grain coarsening in composite matrix. The recrystallization depends on testing temperature and applied strain in case of AZ alloys. However, in present composite, the reinforcement GNPs
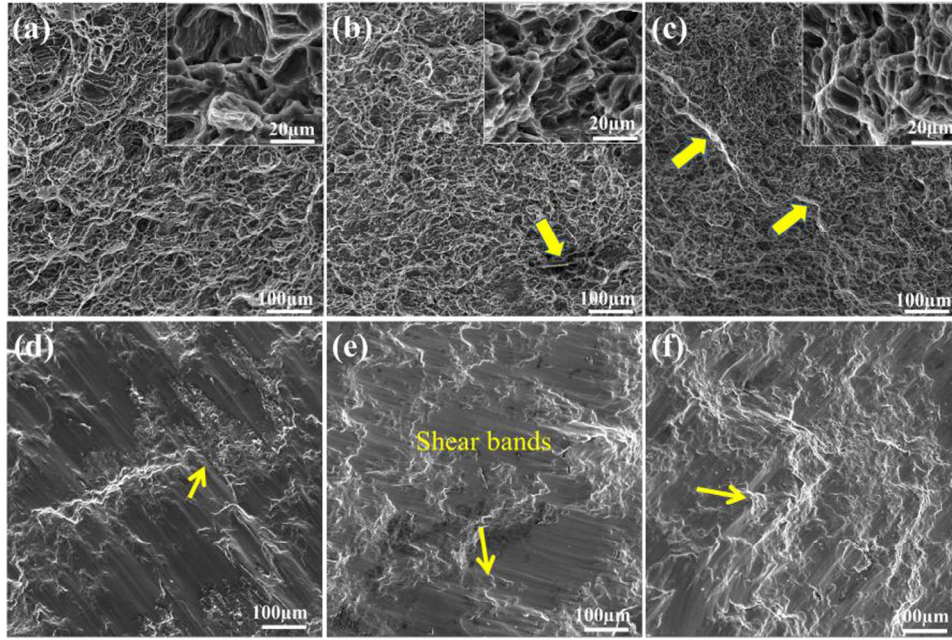
Fig. 7. Tensile fracture surface of extruded (a) AZ31 alloy, (b) AZ31-1.5GNP composite, (c) AZ31-3GNP composite (with insets showing magnified structures); and compressive fracture surface of extruded (d) AZ31 alloy, (e) AZ31-1.5GNP composite, and (f) AZ31-3GNP composite.

propelled the recrystallization process. High temperature flow stress of synthesized materials can be estimated using theoretical models. According to these theoretical models, changes in flow stress depend on testing temperatures. Comparison between theoretical and experimental flow stress can be done using these models. According to Maksoud et al. [27], peak flow stress of material is given as follows [18].

$$\sigma_{FS} = 19.23 \times \sinh^{-1}\left[5.96 \times 10^{-9}\, e^{\left(\frac{152080}{RT}\right)}\right]^{0.44} \tag{2}$$

where σ_{FS} is the peak flow stress, R is molar gas constant, and T is testing temperature. Further, a model was proposed by

Fig. 8. Typical tensile stress–strain curves of AZ31-3GNP composite at different temperatures.

Takuda et al. [28] which can also be used to estimate the peak flow stress, σ_{FS} of materials as given below.

$$\sigma_{FS} = K\varepsilon^n\left(\frac{\varepsilon}{\varepsilon_0}\right)^m \tag{3}$$

where $K = \left(\frac{3.24 \times 10^5}{t}\right) - 406$, $\varepsilon_0 = 1\,s^{-1}$, $n = A\log\left(\frac{\varepsilon}{\varepsilon_0}\right) + B$, $m = \left(\frac{-105}{t}\right) + 0.303$, $t = \frac{T(K)}{1(K)}$, $A = 0.016$, and $B = \left(\frac{62.0}{t}\right) + 0.053$.

In the above equations, K is almost constant and depends on dimensional less temperature, t, ε is strain rate, and T is temperature. The n and m are strain rate sensitivity exponents. A is a constant parameter, while parameter B depends on temperature [18]. Fig. 9(a) shows the effect of testing temperature on flow stress and fracture strain of AZ31-3GNP composite. It can be observed that yield strength decreases and fracture strain increases with increase in temperatures. Fig. 9(b) shows flow stress of AZ31-3GNPs composites calculated by Eqs. (2) and
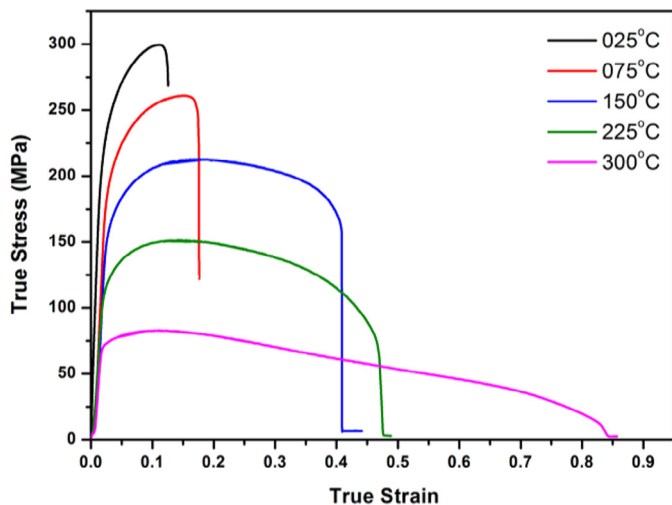
Table 2
High temperature tensile properties of AZ31-3GNP composite.

Temperature (°C)	Tensile properties		
	0.2% YS (MPa)	UTS (MPa)	FS (%)
025	195 ± 4.5	299 ± 6.2	12.56 ± 4.3
075	183 ± 5.2	261 ± 5.4	17.59 ± 5.3
150	144 ± 6.6	212 ± 7.5	40.90 ± 6.9
225	107 ± 4.7	151 ± 8.5	47.53 ± 4.8
300	068 ± 5.7	082 ± 4.9	84.42 ± 7.6

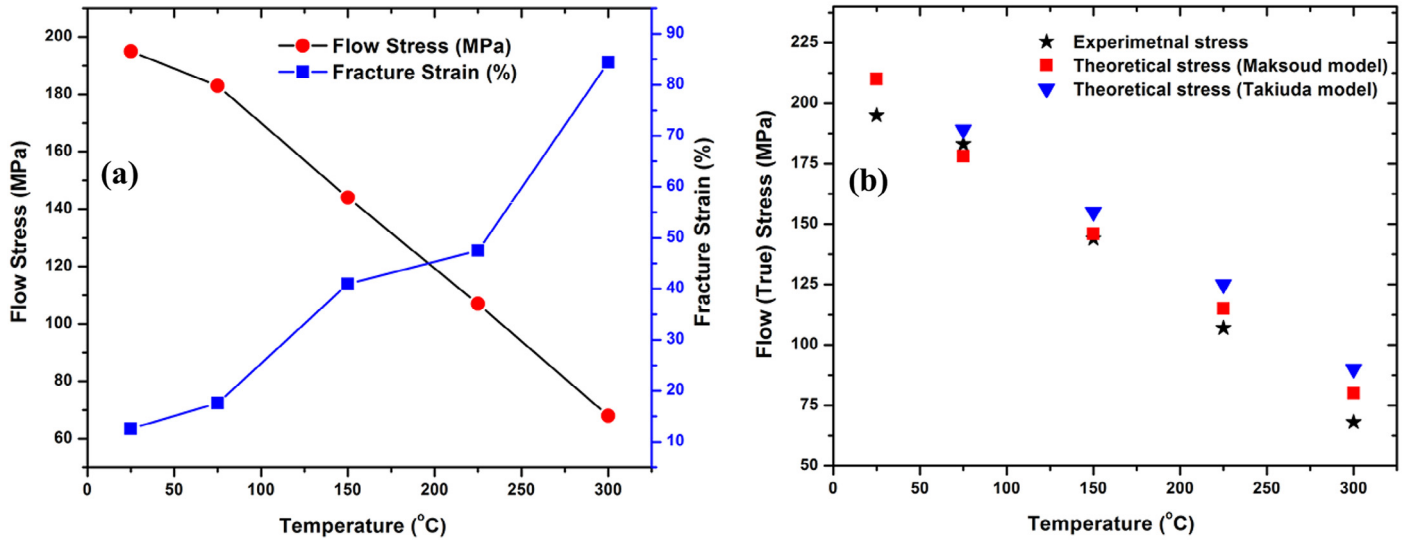YS: Yield strength; UTS: Ultimate tensile strength; FS: Fracture strain.

Fig. 9. (a) Effect of testing temperature on flow stress and fracture strain of AZ31-3GNP composite, and (b) comparison of experimental flow stress with theoretical flow stress.

(3). Comparison was also made with experimental yield stress of composites. It can be seen that theoretical flow stress of composite is approximately equal to experimental flow stress. These predictions show the ability of GNPs in softening of AZ31 alloy matrix at high temperatures.

Fig. 10 shows tensile fracture surfaces of AZ31-3GNPs composites at 25°C, 75°C, 150°C, and 225°C. Careful observations revealed ductile fractures with a lot of dimples and tear ridges. These dimples and tear ridges increases with increase in testing temperatures. Additionally, it can be seen that fractured surfaces at 150°C and 225°C contain micro pores and cracks. This work indicates that GNPs may improve the secondary processing of AZ31 matrix exceptionally [29–31].

4. Conclusions

The AZ31-GNPs composites were successfully synthesized using stir-casting method followed by hot extrusion. The following conclusions can be drawn based on microstructural and mechanical characterizations:

1. The AZ31 magnesium alloys were reinforced with GNP particles. Experimental results revealed the absence of intermetallic phase between reinforcement and matrix. The presence of GNPs affects the formation of $Mg_{17}Al_{12}$ intermetallic phases while solidifying the composite melt. The addition of GNPs has slightly changed the crystallographic texture and grain size of AZ31 alloy.
2. The mechanical testing at room temperature shows significant improvement in micro-hardness. Micro-hardness of alloy increases (both in transverse and longitudinal directions) with increase in GNPs contents. Furthermore, tensile fracture strain and compression yield strength increase remarkably without compromise in mechanical strength. Increased strength of composites is due to changes in basal texture intensity, and efficient load transfer from soft matrix to hard two dimensional GNPs.
3. High temperature tensile testing of AZ31-3GNP composite discovered that GNP led to improved softening with incredible increase in fracture strain of AZ31 matrix. This is caused by complete recrystallization of composite matrix during high temperature testing. The fracture surface analysis revealed that deformation possibly occurs through grain boundary sliding accommodated by diffusional transport. Furthermore, fracture mode of composite changes to ductile mode with increase in testing temperatures.
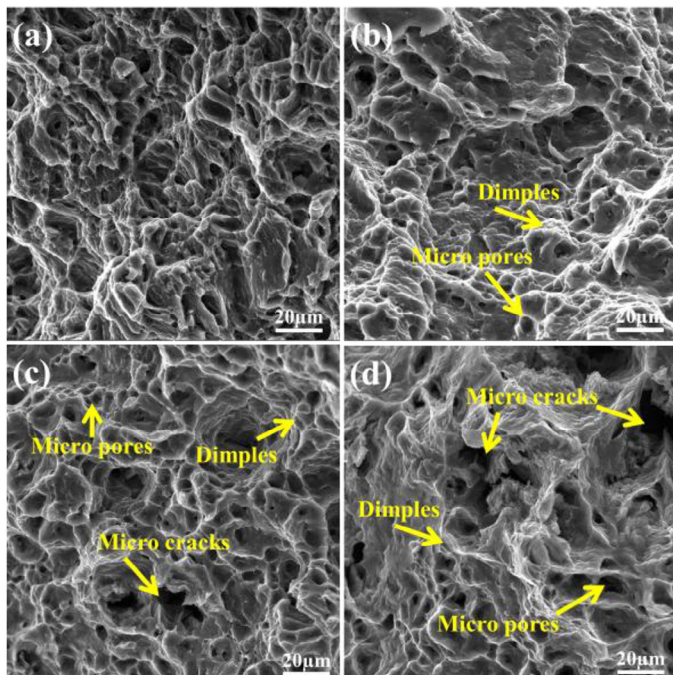

Fig. 10. SEM images of tensile fracture surface of extruded AZ31-3GNP composites tested at (a) 25°C, (b) 75°C, (c) 150°C, and (d) 225°C.

Acknowledgments

References

[1] G.K. Meenashisundaram, M. Gupta, J. Alloys Compd. 593 (2014) 176–183.

[2] G. Han, Z. Wang, K. Liu, S. Li, X. Du, W. Du, Mater. Sci. Eng. 628 (2015) 350–357.

[3] J. Liu, K. Zhao, M. Zhang, Y. Wang, L. An, Mater. Lett. 143 (2015) 287–289.

[4] G.K. Meenashisundaram, M.H. Nai, A. Almajid, M. Gupta, Mater. Des. 65 (2015) 104–114.

[5] H. Watanabe, T. Mukai, M. Sugioka, K. Ishikawa, Scr. Mater. 51 (2004) 291–295.

[6] K. Hu, D.D. Kulkarni, I. Choi, V.V. Tsukruk, Prog. Polym. Sci. 39 (11) (2014) 1934–1972.

[7] S.C. Tjong, Mater. Sci. Eng. 74 (10) (2013) 281–350.

[8] M. Rashad, F. Pan, M. Asif, Mater. Sci. Eng. 649 (2016) 263–269.

[9] M. Rashad, F. Pan, J. Zhang, M. Asif, J. Alloys Compd. 646 (2015) 223–232.

[10] M. Rashad, F. Pan, M. Asif, L. Li, Prog. Nat. Sci. 25 (4) (2015) 276–281.

[11] M. Rashad, F. Pan, Z. Yu, M. Asif, H. Lin, R. Pan, Prog. Nat. Sci. 25 (5) (2015) 460–470.

[12] M. Rashad, F. Pan, A. Tang, M. Asif, S. Hussain, J. Gou, et al., J. Ind. Eng. Chem. 23 (2015) 243–250.

[13] M. Rashad, F.S. Pan, M. Asif, A. Ullah, Mater. Sci. Tech. 31 (12) (2015) 1452–1461.

[14] D. Wenwen, S. Yangshan, M. Xuegang, X. Feng, Z. Min, W. Dengyun, Mater. Sci. Eng. 356 (1–2) (2003) 1–7.

[15] F. Khomamizadeh, B. Nami, S. Khoshkhooei, Metall. Mater. Trans. A 36 (12) (2005) 3489–3494.

[16] S.F. Hassan, M. Paramsothy, Z.M. Gasem, F. Patel, M. Gupta, J. Mater. Eng. Per. 23 (8) (2014) 2984–2991.

[17] S.F. Hassan, M. Paramsothy, F. Patel, M. Gupta, Mater. Sci. Eng. 558 (2012) 278–284.

[18] M. Rashad, F. Pan, D. Lin, M. Asif, Mater. Des. 89 (2016) 1242–1250.

[19] Y.N. Wang, J.C. Huang, Acta Mater. 55 (3) (2007) 897–905.

[20] R.A. Shahani, T.W. Clyne, Mater. Sci. Eng. 135 (1991) 281–285.

[21] X.J. Wang, K. Wu, H.F. Zhang, W.X. Huang, H. Chang, W.M. Gan, et al., Materials Science and Engineering: A 465 (1–2) (2007) 78–84.

[22] E.O. Hall, Proc. Phys. Soc. 64 (9) (1951) 747.

[23] M. Rashad, F. Pan, W. Guo, H. Lin, M. Asif, M. Irfan, Mater. Charact. 106 (2015) 382–389.

[24] Z.Y. Liu, B.L. Xiao, W.G. Wang, Z.Y. Ma, Carbon 50 (5) (2012) 1843–1852.

[25] L. Jiang, Z. Li, G. Fan, L. Cao, D. Zhang, Carbon 50 (5) (2012) 1993–1998.

[26] R.J. Arsenault, N. Shi, Mater. Sci. Eng. 81 (1986) 175–187.

[27] I.A. Maksoud, H. Ahmed, J. Rödel, Mater. Sci. Eng. 504 (1–2) (2009) 40–48.

[28] H. Takuda, T. Morishita, T. Kinoshita, N. Shirakawa, J. Mater. Process. Technol. 164–165 (2005) 1258–1262.

[29] M. Rashad, F. Pan, M. Asif, J. She, A. Ullah, J. Magnes. Alloys 3 (1) (2015) 1–9.

[30] M. Rashad, F. Pan, A. Tang, Y. Lu, M. Asif, S. Hussain, et al., J. Magnes. Alloys 1 (3) (2013) 242–248.

[31] M. Rashad, F. Pan, M. Asif, Mater. Sci. Eng. 644 (2015) 129–136.